frontiers | Frontiers in Environmental Science

TYPE Original Research
PUBLISHED 23 August 2022
DOI 10.3389/fenvs.2022.983430



OPEN ACCESS

EDITED BY
Delong Meng,
Central South University, China

REVIEWED BY
Wei Wang,
Zhengzhou University, China
Shubin Lan,
Northeast Normal University, China

*CORRESPONDENCE
Jianbo Li,
lijianbo3051@163.com

SPECIALTY SECTION
This article was submitted to Toxicology, Pollution and the Environment,
a section of the journal
Frontiers in Environmental Science

RECEIVED 01 July 2022
ACCEPTED 21 July 2022
PUBLISHED 23 August 2022

CITATION
Wang Z, Chen J, Tan J, Lu Z, Wang X, Jianbo Li (2022), The bio-immobilization of Pb(II) induced by the Chlorella–montmorillonite composite in the Ca(II) environment.
*Front. Environ. Sci.* 10:983430.
doi: 10.3389/fenvs.2022.983430



# The bio-immobilization of Pb(II) induced by the *Chlorella*–montmorillonite composite in the Ca(II) environment

Zhen Wang[1,2], Jinhui Chen[3], Jiaqi Tan[1,2], Zijing Lu[1,2], Xizhuo Wang[1,2] and Jianbo Li[4]*

[1]Hubei Key Laboratory of Mineral Resources Processing and Environment, Wuhan University of Technology, Wuhan, China, [2]School of Resources and Environmental Engineering, Wuhan University of Technology, Wuhan, China, [3]School of Public Policy and Management, Tsinghua University, Beijing, China, [4]Instituto de Física de la Universidad Autónoma de San Luis Potosí, San Luis Potosí, Mexico

The clay–microbial consortium is ubiquitous in the soil near the mining area and plays an important role in the transport of heavy metals. In this study, *Chlorella sorokiniana* FK was separated from lead–zinc mine tailings. The montmorillonite–*Chlorella sorokiniana* FK system as a typical case was applied to study Pb(II) biomineralization in the presence of usually co-existent Ca(II) and further reduce the migration and transformation of Pb(II) in the Ca(II) environment. *Chlorella sorokiniana* FK showed good resistance to Pb(II), and the addition of montmorillonite provided a more stable pH environment, which is conducive to the stability of Pb(II)-bearing bio-minerals. Montmorillonite created a low-biotoxicity environment in the overall process, especially less Pb(II) bio-adsorption capacity of individual *Chlorella* to protect the process of mineralization effectively. Batch experiment results also demonstrated that montmorillonite as the formation site of bio-minerals results in dispersed minerals on the surface of *Chlorella* and *Chlorella*–MMT composite, which is beneficial to the survival of *Chlorella*. Moreover, Pb(II)-bearing phosphate minerals tended to form in the Ca(II) environment rather than without Ca(II). This study demonstrated the mechanism of Pb(II) immobilization induced by *Chlorella* in the Ca(II) environment, further presenting a green, sustainable, and effective strategy for Pb(II) bio-immobilization combining clay minerals and microorganisms.

KEYWORDS

**mining area, clay–microbial consortium, montmorillonite, microalgae, bio-immobilization, lead, calcium**

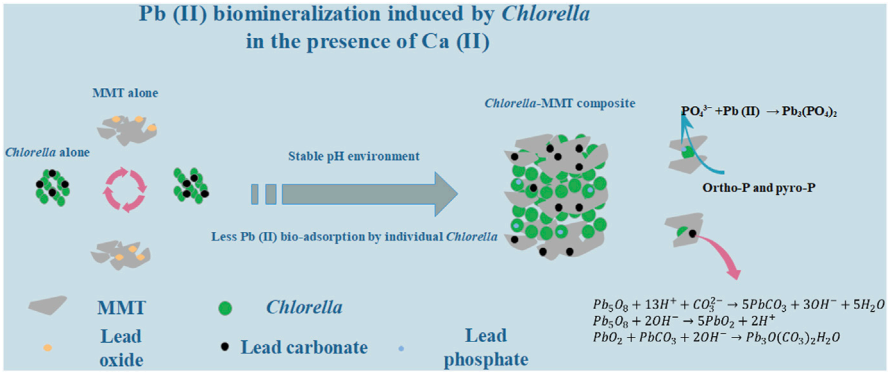


GRAPHICAL ABSTRACT

## 1 Introduction

Mining waste deposits (MWDs) as an important and constant source of lead pollution in the global environment brings a lot of environmental problems (Miler et al., 2022). Heavy metals {including lead [Pb(II)]} continuously leach from long-term stacked tailings and are further transported and transferred through wind, rain, surface water, and groundwater (Senn et al., 2014; Wang et al., 2019; Jiang et al., 2021). The stability and functions of the soil's ecological environment are affected by heavy metal ions seriously (Zhang et al., 2022). Even long after mining stops, river systems near mining sites remain heavily contaminated with heavy metals (Obiri-Yeboah et al., 2021). Taking the Pearl River region as an example (Wu et al., 2020), the Pb(II) content in sediments is two orders of magnitude higher than the corresponding soil background value even downstream of the river. Lead is one of the most hazardous pollutants in nature (Yang et al., 2022), while divalent lead [Pb(II)] is the main form of lead in the environment (Krishnamoorthy et al., 2019), which is extremely bio-toxic (Priyanka et al., 2021) and easy to migrate (Zeng et al., 2022). Pb(II) always positively correlated with Ca(II) concentrations in the mining area (Li et al., 2020). Pb(II) in the environment accumulates in the human body through the food chain (Xu et al., 2021; Gao et al., 2022), and its accumulation shows significant renal toxicity (Bidanchi et al., 2022) and decreases bone strength in humans (Zeng et al., 2016; Osorio-Yanez et al., 2021). Thus, it is a priority to control Pb(II) and its migration in the mining area and further reduce the Pb(II) content in the environment.

In recent years, biomineralization induced by microorganisms has been widely studied as a potential sustainable technique for Pb(II) bio-remediation (Rajasekar et al., 2021; Shan et al., 2021; Yu et al., 2021). The clay–microbial consortium is universal and plays an important role in the transport of heavy metals in the mining area. Compared to conventional methods, the induction of bio-minerals containing Pb(II) can reduce its biotoxicity and migration effectively (Chen et al., 2021). Microalgae as the main producers in the ecosystem are cheap and easy to obtain (Ma et al., 2022; Ummalyma and Singh, 2022) and are widely applied to biological remediation (Cheng et al., 2023). Lee et al. (2014) effectively removed water-soluble radiostrontium by converting it to carbonate through the microalgal photosynthetic process (Lee et al., 2014). However, microalgae cannot survive prolonged periods under the stress of heavy metals (Wu et al., 2016; Li et al., 2022). Moreover, the pH changes mediated by microorganisms, during the overall process of biomineralization (Li et al., 2018), were not conducive to cell breathing and the stability of bio-minerals (Ivanina et al., 2020; Wang et al., 2021). Therefore, it is necessary to create a low toxic and pH-stable environment for the biomineralization process of microalgae.

Montmorillonite (MMT) is a three-layer-structured clay mineral that possesses excellent pH-buffering capacity (Bhattacharyya and Gupta, 2008; Tang et al., 2015) and has been demonstrated to facilitate the formation of cationic bridges between MMT and *Chlorella* in the process of Pb(II) bio-remediation, which effectively decreases the bio-toxicity caused by Pb(II) (Tan et al., 2022). In fact, the formation of cationic bridges was also revealed by Su et al. (2021) to prove the potential protection of *Enterobacter* sp. from Pb(II) stress by clay (Su et al., 2021). Moreover, MMT as clay minerals was demonstrated to provide nutrients and habitats for microorganisms (Li et al., 2019a). Ca(II) in the medium could also effectively reduce the Pb(II) accumulation in biological cells when co-existed with MMT (Hernandez-Garnica et al., 2021). In conclusion, both MMT and Ca(II) show great potential for protecting microbially induced Pb(II) remediation.

In this study, the MMT–*Chlorella sorokiniana* FK system was applied to Pb(II) biomineralization in the presence of Ca(II). The buffering capacity of MMT effectively reduced the pH changes

caused by *Chlorella* and *Chlorella*–MMT composite. The Pb(II) immobilization efficiency induced by different bio-materials was compared to demonstrate the protective mechanism of MMT for algae. Also, the study found that adding MMT reduced the biotoxicity of Pb(II) and Pb(II)-bearing minerals, and MMT was considered the location where Pb(II)-bearing minerals were formed, helping the *Chlorella* survival.

# 2 Materials and methods

## 2.1 Preparation of *Chlorella* and *Chlorella*–MMT composite

In the overall experiment, *Chlorella* was cultured in a BG-11 medium containing 300 mg $NaNO_3$, 36 mg $CaCl_2{\cdot}2H_2O$, 6 mg ammonium citrate monohydrate, 6 mg ammonium ferric citrate, 1 mg EDTA, 2.86 μg $H_3BO_3$, 1.81 μg $MnCl_4{\cdot}H_2O$, 0.222 μg $ZnSO_4{\cdot}7\ H_2O$, 0.39 μg $NaMoO_4{\cdot}5H_2O$, 0.079 μg $CuSO_4{\cdot}5H_2O$, 0.050 μg $CoCl_2{\cdot}6\ H_2O$, and 40 mg $K_2HPO_4$ in 1 L sterile distilled water. Moreover, microalgae were cultivated at 25°C with a light–dark cycle of 14/10 h under artificial radiation of 200 μmol proton$^{-1}$m$^{-2}$s$^{-1}$. Furthermore, the microalgae cells were obtained at the stationary phase and washed three times with ultrapure water for subsequent experiments. *Chlorella* used in this experiment was isolated from Fan Kou lead–zinc mine tailings, Shaoguan City, and it is strong homology with *Chlorella sorokiniana* identified based on 18 S rDNA profiles as described by Koloren et al. (2016). The montmorillonite in this study was obtained from Ningcheng County, Chifeng City (Inner Mongolia, China), was sterilized under ultraviolet light for half an hour, and was further composited with *Chlorella*. Next, *Chlorella* and montmorillonite were thoroughly mixed in the ratio of 1:0, 1:1, and 1:5 (*Chlorella*: MMT, W/W) and stirred for 24 h. In addition, total microalgal biomass dry weight was controlled to 0.272 g/L.

## 2.2 Adsorption and mineralization

The concentrations of Pb(II) and Ca(II) in *Chlorella* and *Chlorella*–MMT composite suspension were measured to demonstrate the improved Pb(II) removal efficiency with MMT, and the influence of Ca(II) in the overall process was revealed. In this study, Pb(II) stock solution (15 g/L) and Ca(II) stock solution (1 mol/L) were prepared with $Pb(NO_3)_2$ and $CaCl_2$. At the sampling time, 10 ml Pb(II) and Ca(II) stock solutions were added to the 1 L composite system. The initial concentration of Pb(II) was set at 150 mg/L, while the initial concentration of Ca(II) was 10 mmol/L. After all, a certain volume of suspension was taken and centrifuged at 5,000 rpm for 5 min. The centrifuged supernatant was used to determine the concentration of Pb(II) and Ca(II). Furthermore, the centrifuged sediment was freeze-dried and stored at −18°C for subsequent experiments.

## 2.3 Measurements

The atomic absorption spectrometer (Agilent 240FS flame atomic absorber) was used to detect the concentrations of Pb(II) and Ca(II). The composition analysis of crystalline materials was compiled by X-ray diffraction (XRD) (Zhang et al., 2013), and particular attention was paid to the parts of the clay mineral surface containing Pb(II) and Ca(II). The Bruker D8 advance diffractometer was used for diffraction analysis of mineral crystals on the surface of *Chlorella* and *Chlorella*–MMT composites under different conditions in this study. It is mainly used for the analysis of clay minerals (referring to montmorillonite) and minerals containing Pb(II)/Ca(II) on the surface of *Chlorella* and *Chlorella*–MMT composite. Scan diffraction angles were set from 10° to 80° at a scanning speed of 2°min. Furthermore, the effects of different montmorillonite contents and dissolved Ca(II) on the biologically induced formation of Pb-bearing minerals were explored. The laser Doppler electrophoresis technique using a Malvern Zetasizer (NanoZS90, United Kingdom) was used to investigate the zeta potential of *Chlorella*, montmorillonite, and their composites (1:1 and 1:5 *Chlorella*/MMT mass ratios) at a pH range of 5.0–7.5. The scanning electron microscope (SEM) and energy-dispersive spectrometer (EDS) (Phenom 6.0, Thermo Fisher Scientific, United States) were used to characterize the distribution of Pb(II)/Ca(II) on *Chlorella*, MMT, and their composite. Transmission electron microscopy and select area electrical diffraction (TEM-SAED, JEM-2100F) images of the samples were taken to reveal the morphology and main composition of mineral particles on the *Chlorella*–MMT composite. Fourier transform infrared spectroscopy (FT-IR, Thermo Scientific) analysis of *Chlorella*, MMT, and their composite (*Chlorella*: MMT = 1:1) ranged from 400 to 4,000 cm$^{-1}$, further investigating functional groups involved in Pb(II)/Ca(II) adsorption and mineralization. X-ray photoelectron spectroscopy (Thermo Scientific ESCALAB 250Xi) measurements were performed to explain the change of elemental forms of C 1s, O 1s, and P 2p before and after Pb(II)/Ca(II) loaded, and the main elemental forms of Pb 4f, Ca 2p, Si 2p, and Al 2p after Pb(II)/Ca(II) loaded.

# 3 Results and discussion

## 3.1 Mineralization of Pb(II)

### 3.1.1 The structure of Pb(II)-bearing minerals

In this study, Pb(II) in the environment adsorbed by *Chlorella*, MMT, and their composite further formed stable

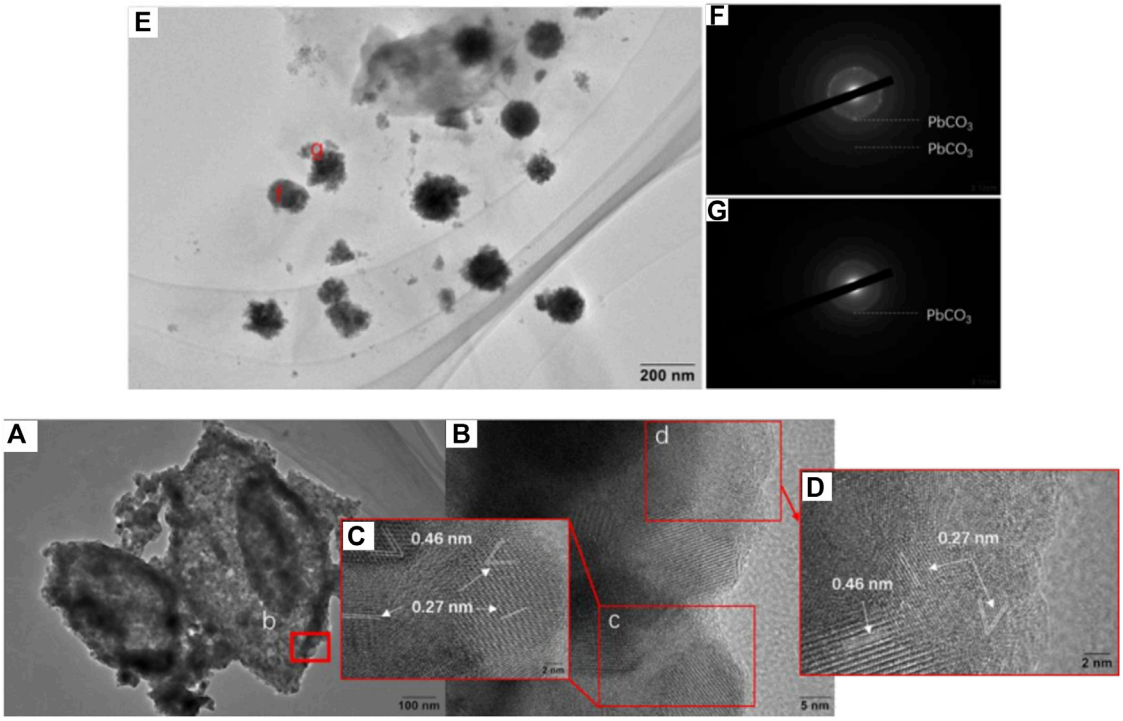


FIGURE 1
**(A)** HRTEM images of *Chlorella*–MMT (1:1) composites after Pb(II)/Ca(II) loaded. **(B–E)** Enlarged images of the corresponding positions. **(F,G)** SAED pattern of the corresponding position.

metal minerals induced by microorganisms (Cheng et al., 2022). The structure of Pb(II)-bearing minerals induced by *Chlorella* was successfully observed on the *Chlorella*–MMT (1:1) composite via TEM and SAED. After 167 h Pb(II)/Ca(II) loaded, a single *Chlorella* cell was completely encapsulated by mineral particles. The minerals on the surface of *Chlorella* showed a collection of nanospherical particles with an average size of 10 nm in Figure 1 (a). Combing the SAED patterns in Figures 1F,G, Pb(II)-bearing minerals showed the typical aggregation of polycrystalline nanoparticles. The d-spacing of 3.23 and 7.38 Å matches well with the (202) and (310) planes of $PbCO_3$, respectively. A wide amorphous separation ring observed at the periphery showed the amorphous-edged nanoparticles (Liu et al., 2019). As shown in Figure 1A, the lattice structures of parts c and d of region b were magnified and observed, and the lattice spacings equal to 0.46 and 0.27 nm correspond to the (200) and (400) planes of $PbCO_3$, respectively. Pb(II) was successfully loaded as carbonate Pb(II)-bearing minerals, which showed a well-structured crystal. The formation of $PbCO_3$ and other possible minerals on the surface of the *Chlorella*–MMT composite is necessary to investigate the process of biomineralization.

### 3.1.2 Bio-mineral compositions

XRD was used to characterize the mineral compositions of polycrystals under different treatments. Bio-minerals on the surface of *Chlorella*, MMT, *Chlorella*–MMT composite (1:1), and *Chlorella*–MMT composite (1:5) after Pb(II)/Ca(II) loaded were characterized to investigate the biomineralization induced by *Chlorella*. There was a broadening but less intense diffraction peak at 20 as in Figure 2A, which shows a distinctly amorphous shape without the diffraction peak of mineral crystals (Samsudin and Saadiah, 2018). The XRD patterns of MMT before and after Pb(II) loaded are shown in Figures 2B–D, and the reflections at 2θ = 22.0, 22.9, 23.4, 32.3, and 24.9° shown in Figure 2D were assigned to $PbCl_2$ as chemical precipitate, which formed through the reaction of Cl-ion and Pb(II) in this solution (An and Dultz, 2008). Meanwhile, the reflections at 2θ = 21.0, 36.3, 41.8, and 46.4° were assigned to $Pb_5O_8$, and Pb(II) successfully broke the Si-O-Si bond and remained in the oxide matrix, surrounded by the O ion (Liu et al., 2014). Figures 2C–E show the XRD pattern of the *Chlorella*–MMT (1:1) composite before and after Pb(II)/Ca(II) loaded, respectively. Before Pb(II)/Ca(II) loaded, the reflections in the XRD pattern at 2θ = 17.8, 19.8, 23.6, 54.1, and 61.8° were completely assigned to MMT, while the reflections

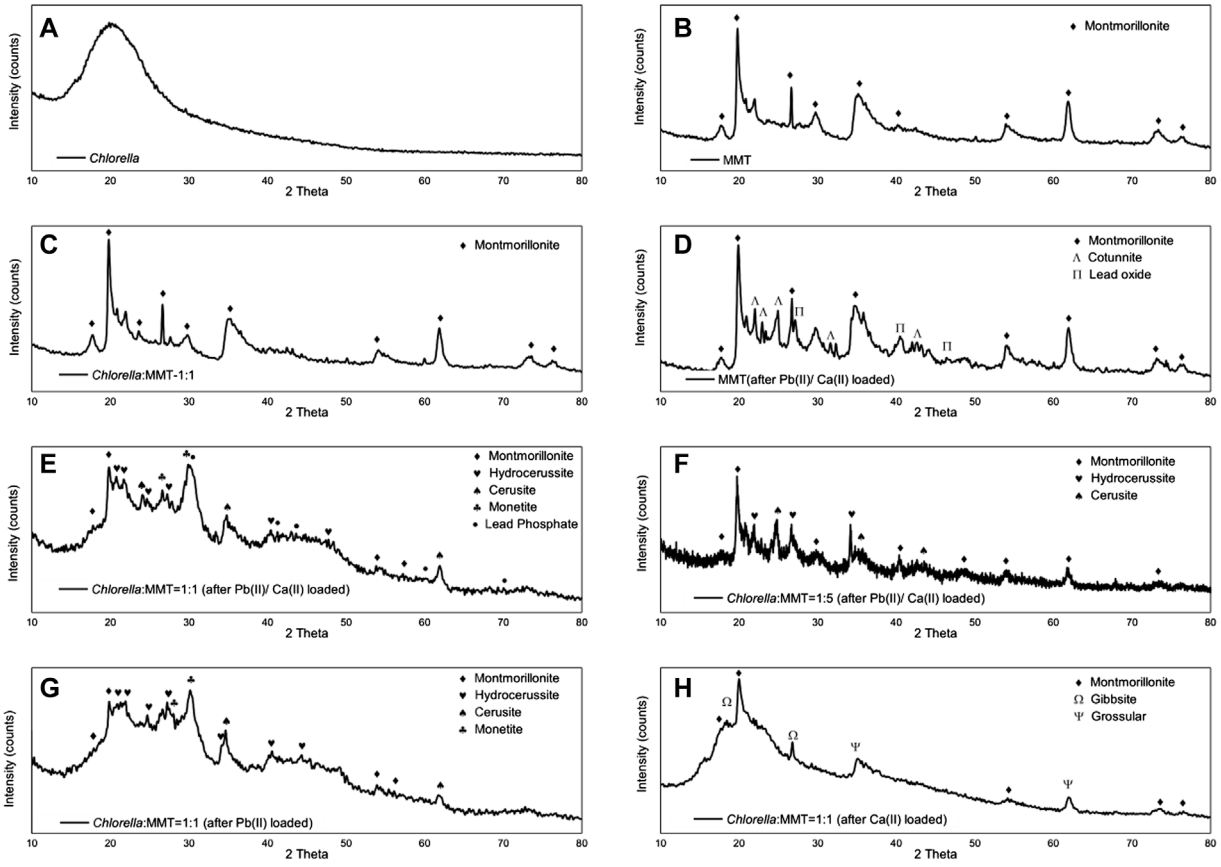


FIGURE 2
XRD spectra of **(A)** *Chlorella*; **(B)** MMT; **(C)** *Chlorella*: MMT = 1:1; **(D)** MMT (after Pb(II)/Ca(II) loaded); **(E)** *Chlorella*: MMT = 1:1 (after Pb(II)/Ca(II) loaded); **(F)** *Chlorella*: MMT = 1:5 (after Pb(II)/Ca(II) loaded); **(G)** *Chlorella*: MMT = 1.1 (after Pb(II) loaded); and **(H)** *Chlorella*: MMT = 1:1 [after Ca(II) loaded].

at 2θ = 19.8, 20.9, 36.0, 40.3, 54.1, and 73.2° were assigned to $Pb_3O(CO_3)_2H_2O$, and the XRD pattern at 2θ = 20.8, 34.6, 43.4, and 61.7° belong to $PbCO_3$ after Pb(II)/Ca(II) loaded. The decreased pH shown in Figure 3 may be caused by the production of carbonates and $CO_2$ in this study, with which the formation of $Pb_3O(CO_3)_2H_2O/PbCO_3$ is mainly associated. $Pb_3O(CO_3)_2H_2O/PbCO_3$ did not form on the surface of MMT alone, which suggests that the bio-minerals are mainly induced by *Chlorella*. $Pb_3O(CO_3)_2H_2O$ observed on the surface of the *Chlorella*–MMT composite was mainly formed by $PbO_2$ (Eq. 3) (Cowley, 1956), while $PbCO_3$ and $PbO_2$ were formed by $Pb_5O_8$ (Eqs 1, 2) (Winning et al., 2017). Pb(II) first entered MMT and further formed Pb(II)-bearing minerals induced by *Chlorella*, and this process facilitated the formation sites of $Pb_3O(CO_3)_2H_2O/PbCO_3$ transfer to MMT. MMT as the formation site of Pb(II)-bearing minerals is conducive to reducing the bio-toxicity of Pb(II)-bearing minerals to *Chlorella*.

$$Pb_5O_8 + 13H^+ + CO_3^{2-} \rightarrow 5PbCO_3 + 3OH^- + 5H_2O \quad (1)$$

$$Pb_5O_8 + 2OH^- \rightarrow 5PbO_2 + 2H^+ \quad (2)$$

$$PbO_2 + PbCO_3 + 2OH^- \rightarrow Pb_3O(CO_3)_2H_2O \quad (3)$$

In addition, the mineral compositions on the surface of the *Chlorella*–MMT composite (1:1) after Pb(II) loaded and after Ca(II) loaded were compared to demonstrate the influence of Ca(II). Interestingly, the Pb(II)-bearing phosphate minerals were found in the presence of Ca(II). The reflections at 2θ = 30.3, 41.1, 44.3, 60.5, and 70.2° were assigned to $Pb_3(PO_4)_2$ as shown in Figure 2E. In the process of Pb(II) remediation, *Chlorella* not only induced the formation of carbonate minerals but also phosphate minerals, whereas phosphate minerals are more stable than carbonate minerals in an acid environment. More stable Pb(II)-bearing minerals like phosphate minerals also is more conducive to reducing the migration of Pb(II) in the mining area. Similarly, we compared the results of the *Chlorella*–MMT (1:1) composite with the

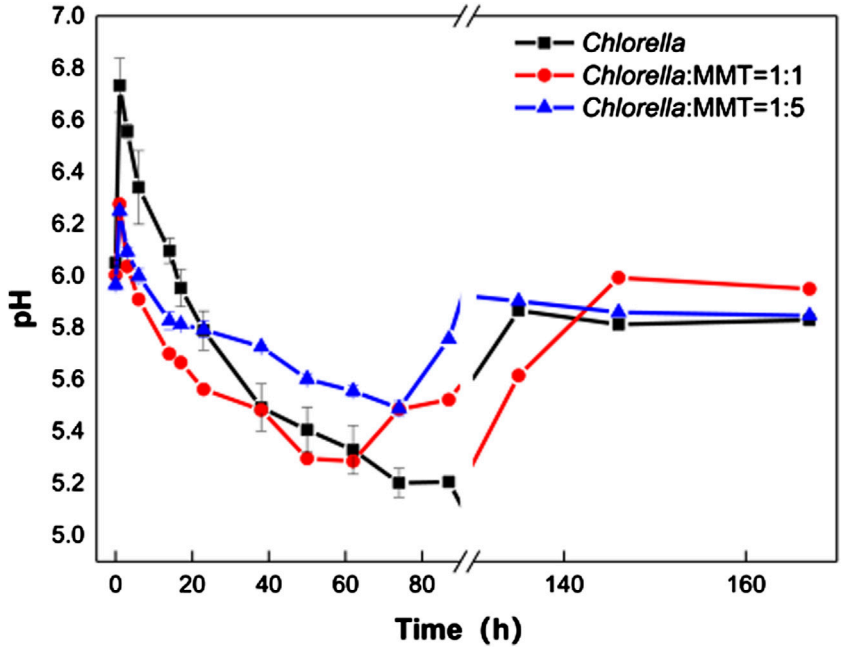


FIGURE 3
pH changes in *Chlorella* and *Chlorella*: MMT = 1:1 and 1:5 composite suspension.

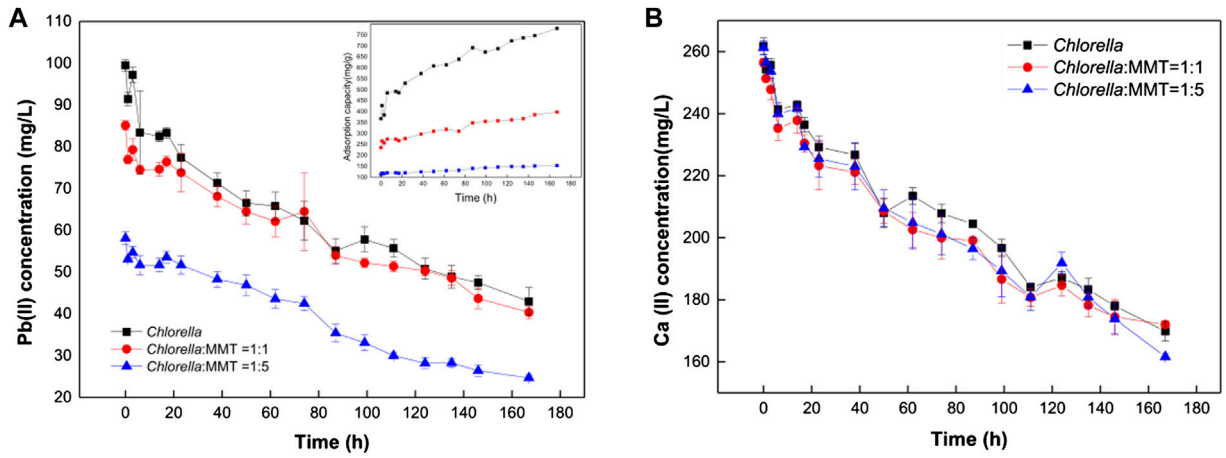


FIGURE 4
Variation of Pb(II) concentration **(A)** and Ca(II) concentration **(B)** in *Chlorella* and *Chlorella*–MMT (1:1 and 1:5) composite suspension.

X-ray diffraction pattern of the *Chlorella*–MMT (1:5) composite. After Pb(II)/Ca(II) loaded, both $Pb_3O(CO_3)_2H_2O$ and $PbCO_3$ were detected rather than phosphate minerals. Phosphate minerals are mainly formed on the surface of *Chlorella*. Conversely, excess MMT as the formation site was not conducive to this process. The comparison of the results is shown in Figures 2G,H. When only Pb(II) is loaded, minerals on *Chlorella*–MMT (1:1) composite is mainly $Pb_3O(CO_3)_2H_2O$ and $PbCO_3$. Conversely, the XRD diffraction peaks at 2θ = 36.6, 37.9, 41.8, and 63.8° and 2θ = 36.6, 39.4, and 50.6° in Figure 2H were assigned to Al $(OH)_3$ and $Ca_3Al_2(SiO_4)_3$, respectively. *Chlorella* did not induce Ca(II) carbonate biomineralization in the absence of Pb(II) stress.

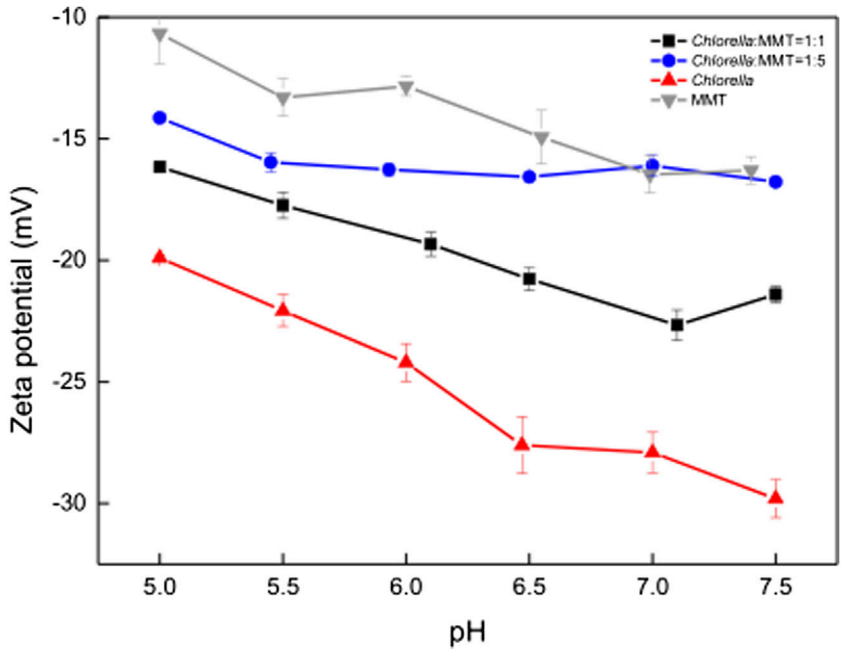


FIGURE 5
Zeta potential of MMT, *Chlorella*, *Chlorella*–MMT composite (1:1), and *Chlorella*–MMT (1:5) composite.

## 3.2 Pb(II) remediation in coexistence with Ca(II)

### 3.2.1 pH stability

In Figure 3A, Pb(II) continues to decrease instead of re-release to the environment after being adsorbed by materials. The biomineralization process induced by *Chlorella* is always associated with the variation of pH in the environment. Therefore, it is necessary to investigate the role of biomineralization in the variation of pH values mediated by *Chlorella*. In fact, the acidification of the solution in the mineralization process could lead to the re-release of Pb(II)-bearing minerals, especially carbonate Pb(II)-bearing minerals. The pH variations in the three groups are shown in Figure 3. The Pb(II) immobilization induced by *Chlorella* alone caused larger environment pH changes, which is not conducive to the stability of Pb(II)-bearing minerals, especially carbonate Pb(II)-bearing minerals. At the same time, the addition of MMT from 1:1 to 1:5 in the group of *Chlorella*–MMT composite resulted in a more flatted pH change than *Chlorella* alone. In detail, the variation of pH mediated by *Chlorella* alone changed from 5.07 to 6.73, while the variation of pH mediated by *Chlorella*–MMT (1:1 and 1:5) composites ranged from 5.23 to 6.27 and 5.49 to 6.25, respectively, as shown in Figure 3. $CO_2$ released from *Chlorella* in the presence of Pb(II) stress caused pH to continuously decline (Carfagna et al., 2013), further inducing the formation of Pb(II)-bearing carbonate minerals mentioned in Figure 1 and Figure 2. The increasing MMT content results in an environment with higher or lower pH values at the same periods in the process of mineralization. The increasing pH within 1 h is possibly caused by the assimilation of nitrate contained in the medium (Wang et al., 2016). MMT has provided a stable environment for Pb(II) remediation induced by *Chlorella*, while the pH-buffering capacity of MMT is favorable for reducing the release of Pb(II) in minerals.

### 3.2.2 Pb(II)/Ca(II) concentration

In the overall bio-remediation process, the concentration of Pb(II) and Ca(II) continues to decrease instead of removal stops after adsorption saturation as shown in Figure 4. There is a brief recovery of Pb(II) concentration that can be observed at 1–3 h, which is associated with increasing pH consistent with that pH ranging from 5.0 to 6.5 conducive to the adsorption of Pb(II) (Slaveykova and Wilkinson, 2003). The Pb(II) concentration in the group of *Chlorella*–MMT composite (1:1 and 1:5) was 1.06 times and 1.64 times as much as that in *Chlorella* alone on average. Moreover, Pb(II) in the environment will be continuously remediated by *Chlorella*, MMT, and *Chlorella*–MMT composite, not only adsorbed but also formed Pb(II)-bearing minerals induced by *Chlorella*. MMT as the formation site of Pb(II)-bearing minerals mentioned in Figure 2 also effectively reduces the concentration of Pb(II) and further protects the process of biomineralization induced by *Chlorella* in this way. The adsorption capacity of *Chlorella* was 1.86 times and

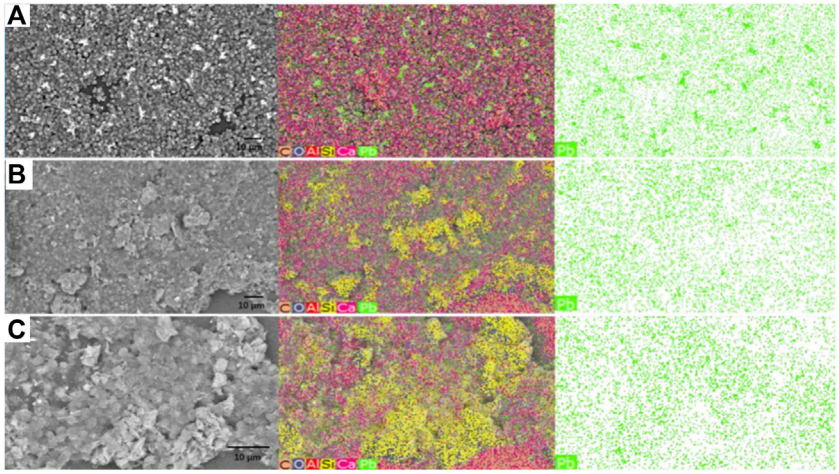


FIGURE 6
SEM-EDS image of **(A)** *Chlorella*, **(B)** *Chlorella*–MMT (1:1), and **(C)** *Chlorella*–MMT (1:5)

4.44 times as much as that of the *Chlorella*–MMT composite (1:1 and 1:5), respectively. MMT reduces the stress of Pb(II) to *Chlorella* in solution effectively. Generally, MMT has created a low-biotoxicity environment and led to less Pb(II) bio-adsorption by individual *Chlorella*. However, the addition of MMT seems to exhibit few significant differences in Ca(II) adsorption, and the variation of Ca(II) in the three groups is almost alike, which suggests that decreased Ca(II) is mainly associated with *Chlorella* rather than MMT. The uptake of Ca(II) by *Chlorella* is conducive to reducing intracellular Pb(II) accumulation (Li et al., 2019a). These are beneficial for the survival of *Chlorella* and further facilitated the biomineralization induced by *Chlorella*.

### 3.2.3 Less bio-toxicity of Pb(II) and Pb(II)-bearing minerals

The clay–microbial consortium, *Chlorella*, MMT, and *Chlorella*–MMT composite exhibited significant electronegativity in the pH range from 5.0 to 7.5, while Figure 3 indicates that pH changed from 5.0 to 6.8 during the overall process. The results in Figure 5 showed that *Chlorella* had more Pb(II)-binding sites on its surface than MMT, which investigated the effect of negatively charged MMT on the whole process to illustrate the decrease of Pb(II) around *Chlorella*. The zeta potential of *Chlorella* changed from −19.9 mV to −29.8 mV, whereas that of MMT changed from −10.7 mV to −16.3 mV as shown in Figure 5. The increased MMT content led to a lower Pb(II)-binding capacity of the *Chlorella*–MMT composite. These results demonstrated that compounding *Chlorella* with MMT is beneficial to reducing the surface adsorption capacity of individual *Chlorella*, which also corresponds to the lower Pb(II) adsorption capacity exhibited by the *Chlorella*–MMT composite in Figure 4A and further facilitates Pb(II) mineralization induced by *Chlorella* in the presence of Ca(II).

In addition, the SEM-EDS images of *Chlorella* and *Chlorella*–MMT (1:1) composite are shown in Figures 6A–C, respectively. Combining the crystal positions with Pb(II) distribution sites as shown in Figure 6, Pb(II) was successfully loaded on the surface of *Chlorella* and *Chlorella*–MMT composites and also demonstrated the position of Pb(II)-bearing minerals induced by *Chlorella* and *Chlorella*–MMT composites. In detail, the formed Pb minerals observed on the *Chlorella* cells were larger and more clustered, which is conducive to killing the *Chlorella* cells rather than protecting them because the larger Pb(II) minerals are easier to reduce the nutrition exchange for *Chlorella* (Rahman and Singh, 2020). Moreover, only small crystals were observed in the group of *Chlorella*–MMT composites (1:1 and 1:5), suggesting that the addition of MMT led to more dispersed minerals and was beneficial for the *Chlorella* by persistently inducing the formation of Pb(II) minerals.

## 3.3 Mechanism of Pb(II) bio-remediation

### 3.3.1 FT-IR

Pb(II) adsorbed is always associated with the functional groups on the surface of *Chlorella*, MMT, and *Chlorella*–MMT composites. Furthermore, the functional groups involved in the process of bio-remediation were revealed by the FT-IR spectra of MMT, *Chlorella*, and their composites (1:1) before and after Pb(II)/Ca(II) loaded. In Figure 7A, the characteristic peaks at 3622.08(Al-OH) and 3421.38(H-OH) $cm^{-1}$ were assigned to -OH vibration of MMT and water molecules, respectively. For *Chlorella*, the peaks at 3308.20 and 1,394.41 $cm^{-1}$ in Figure 7B were attributed to -OH stretching vibrations of carbohydrates,

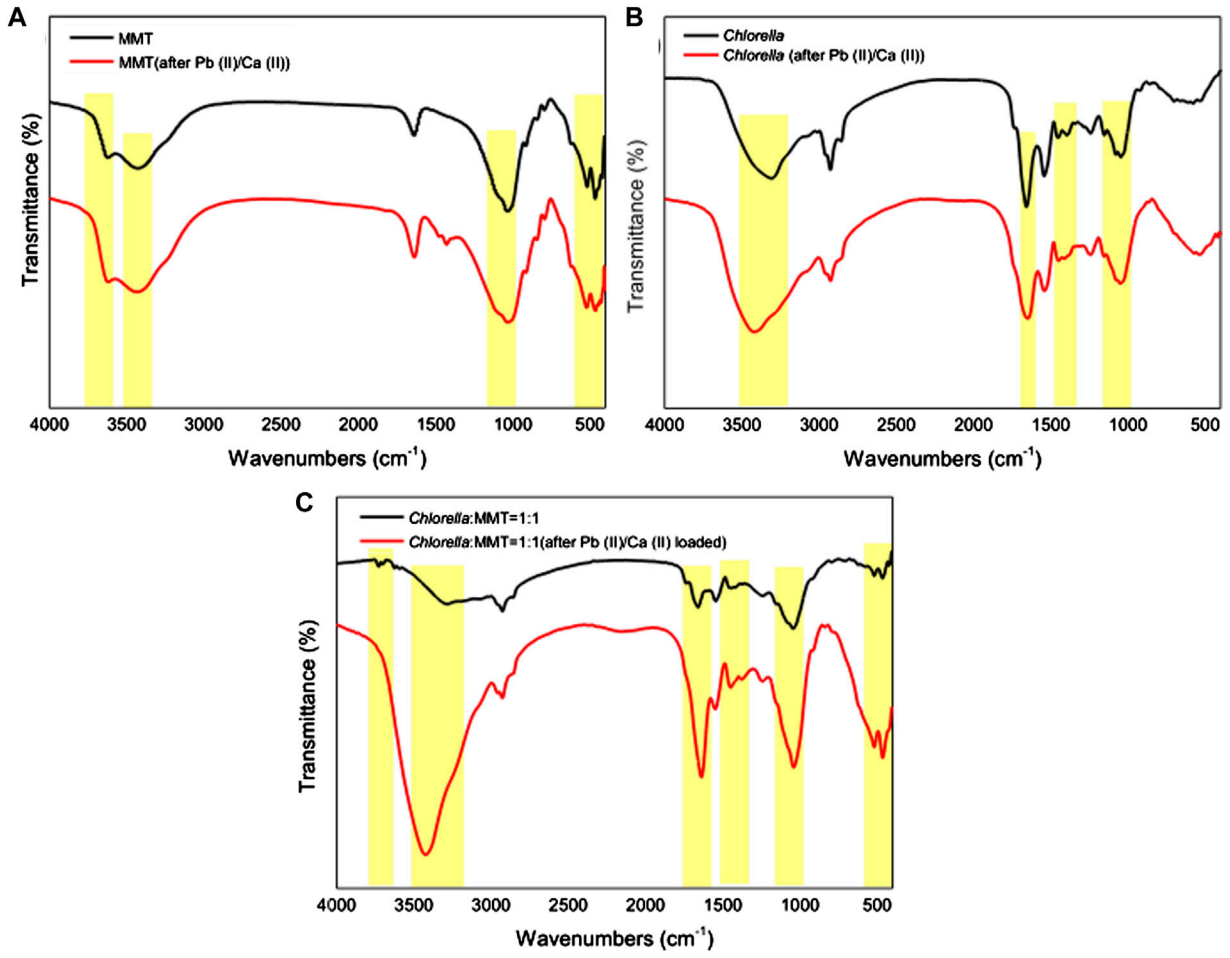


FIGURE 7
FT-IR spectra of **(A)** MMT, **(B)** *Chlorella*, and **(C)** *Chlorella*–MMT (1:1) composite before and after Pb(II)/Ca(II) loaded.

proteins, and lipids (Li et al., 2019b). As for the *Chlorella*–MMT composite, the peaks at 1,659.68 and 1,446.23 $cm^{-1}$ belong to COO- stretching, whereas the peaks at 1,649.30 and 1,452.83 $cm^{-1}$ in Figure 7B are also due to COO- stretching, which proved that Ca(II) and Pb(II) coordinate with the carboxylic acid group in a bidentate bridging manner (Ibrahim et al., 2011). For MMT and *Chlorella*–MMT composites, the assignments for the 518.32 and 518.06 $cm^{-1}$ bands are Si-O and Si-O-Al stretching, respectively (Kumar and Lingfa, 2020). There is a medium sharp band at 465.88 and 466.10 $cm^{-1}$, which is allocated due to Si-O-Si stretching. The microstructure of montmorillonite changed because of the adsorption and biomineralization process of Pb(II)/Ca(II). The disappearance of the peak at 3728.53 $cm^{-1}$ (Al-OH) in Figure 7C could be also due to the ion exchange of MMT to adsorbed Ca(II)/Pb(II). The peaks at 1,047.24 and 1,044.46 $cm^{-1}$ were assigned to asymmetric stretching modes of P-O bonds in $(PO_4)^{3-}$ units (Nzaba Madila et al., 2022), shifted from 1,047.24 and 1,044.46 $cm^{-1}$ to 1,047.97 and 1,040.74 $cm^{-1}$ in Figures 7B,C due to the formation of phosphate minerals, which was induced by *Chlorella* after Pb(II)/Ca(II) adsorption. The shifted functional groups are summarized in Supplementary Table S1.

### 3.3.2 XPS

The XPS of the *Chlorella*–MMT (1:1) composites in Figure 8 was used to elucidate the Pb(II)/Ca(II) immobilization mechanism, especially the formation of Pb(II)-bearing minerals and the widely differing P chemical shifts. Supplementary Tables S2A, B show the surface elemental composition and relative data of the *Chlorella*–MMT composite detected from XPS analyses. The survey XPS spectrum of the *Chlorella*–MMT composite is shown in Figure 8A, which also revealed that Pb(II) was successfully loaded onto the *Chlorella*–MMT composite after Pb(II)/Ca(II) was contacted. In addition, Figures 8B–D show C 1s, O 1s, and P 2p XPS spectra in *Chlorella*–MMT composites before and after Pb(II)/Ca(II) loaded, respectively. The peaks at 284.80, 286.32, 288.02, and 289.05 eV in Figure 8B belong to C-C/C-H, C-O, C=O, and O=C-O, which could be assigned to aromatic, hydroxyl, alcohol, carboxyl,

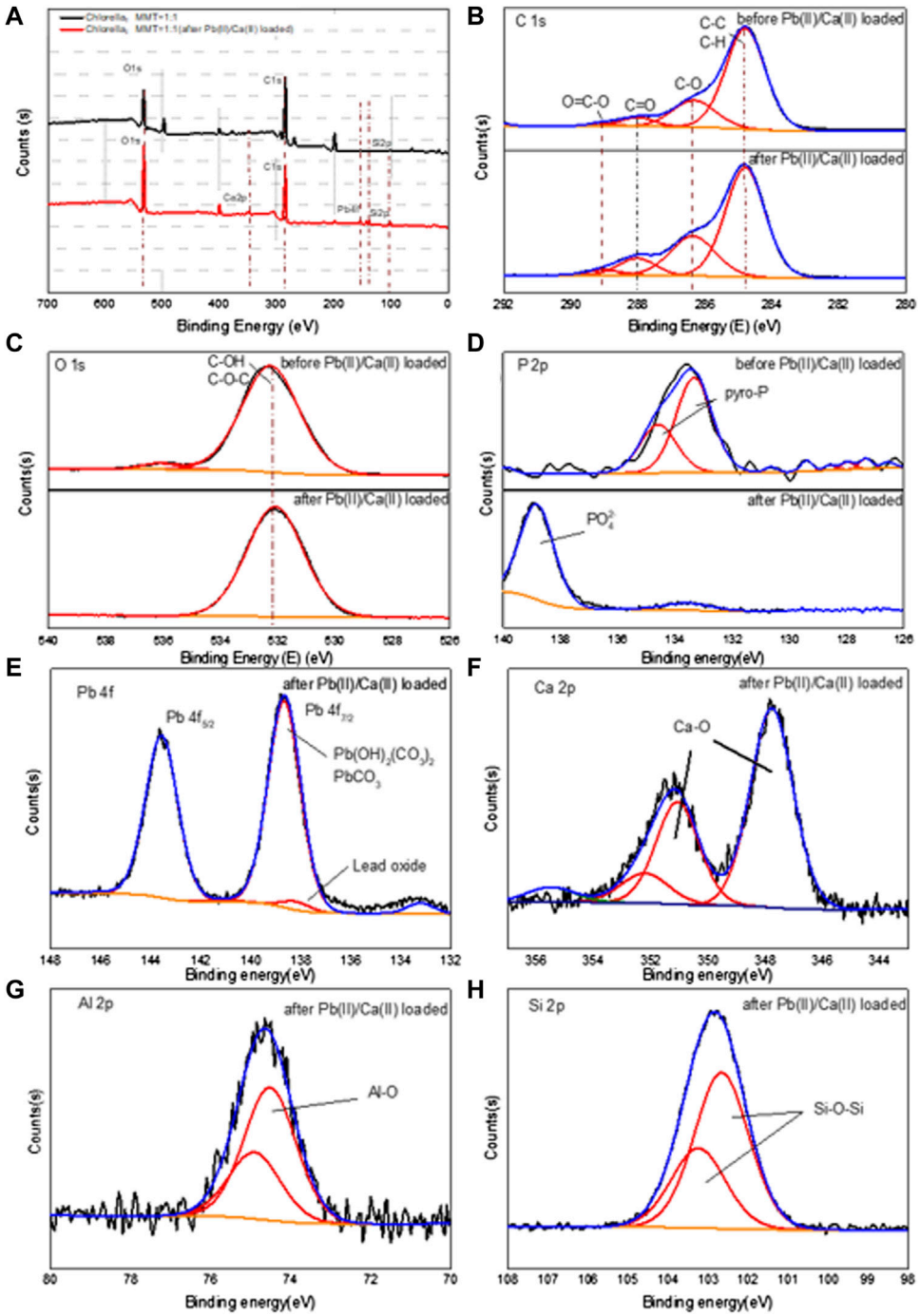


FIGURE 8
XPS spectra of full spectrum **(A)**, C ls **(B)**, O 1s **(C)**, and P 2p **(D)** before and after Pb(II)/Ca(II) loaded; Pb 4f **(E)**, Ca 2p **(F)**, Al 2p **(G)**, and Si 2p **(H)** after Pb(II)/Ca(II) loaded on *Chlorella*–MMT (1:1) composite.

and ketone groups of *Chlorella*, respectively (Tan et al., 2022). In Figure 8C, the peaks at 532.25 eV assigned to C-OH (Huang et al., 2019) were consistent with the results in Figures 8A–C. The changes in peak area and binding energy demonstrated that carboxyl and hydroxyl groups played key roles in the process of Pb(II) adsorbed by the *Chlorella*–MMT composite. In addition, the peaks at 133.33 and 134.58 eV were attributed to the overlapped peaks of orthophosphate (ortho-P) and pyrophosphate (pyro-P) (Qian et al., 2014), which were widely distributed on the surface and inside of *Chlorella* (Kang et al., 2018), respectively. After Pb(II)/Ca(II) loaded,

the original peaks disappeared and a new single peak at 139 eV appeared that belongs to $PO_4^{3-}$ (Nzaba Madila et al., 2022). Thus, the widely differing P chemical shifts among orthophosphate and pyrophosphate species are readily distinguishable after Pb(II)/Ca(II) is loaded. Ortho-P and pyro-P being hydrolyzed into $PO_4^{3-}$ by various phosphatases may be related to the increase in phosphatase activity caused by Ca(II) (Zhu et al., 2018; Hernandez-Garnica et al., 2021). $Pb_3(PO_4)_2$ was formed further, which was consistent with the results in Figure.8E.

After Pb(II)/Ca(II) loaded, Pb 4f, Ca 2p, Al 2p, and Si 2p XPS spectra in the *Chlorella*–MMT (1:1) composite are shown in Figures 8E–H. The Pb 4f peak can be fitted to two components centered at 138.67 eV and 143.57 eV, which were attributed to $PbCO_3$/$Pb_3O(CO_3)_2H_2O$, respectively, while there is a single peak at 139 eV that was assigned to lead oxide, corresponding to the results shown in Figure 8E. Also, two distinct peaks for Ca 2p were attributed to Ca 2p3/2 (347.76 eV) and Ca 2p1/2 (351.34 eV) in Figure 8 (h). The binding energy interval between Ca 2p3/2 and Ca 2p1/2 is 3.58 eV, which indicated the spin-orbit splitting (binding energy separation) related to Ca-O ($CaCO_3$) (Dhankhar et al., 2017; Saisopa et al., 2020). As shown in Figure 8G, the main peak in the Al 2p spectrum was located around 74.32 and 74.71 eV, which was assigned to the Al–O ($Al_2O_3$) bond in the composite after Pb(II) loaded; the presence of the small shoulder in the higher energy region of Al 2p spectra may be caused by Pb(II)/Ca(II) doping (Figueiredo et al., 2011). In Figure 8H, the *Chlorella*–MMT (1:1) composites showed a strong Si 2p peak at 102.46 and 103.04 eV after Pb(II)/Ca(II) loaded, which corresponded to the Si-O-Si bond of MMT. Similar results were also obtained in the XRD diffraction pattern and FT-IR spectra.

## 4 Conclusion

This study revealed the protective mechanism of MMT for the biomineralization of Pb(II) induced by *Chlorella*: one is providing a more stable pH environment, which is conducive to the stability of Pb(II)-bearing carbonated minerals. Second is beneficial to creating a low-biotoxicity environment and less Pb(II) bio-adsorption capacity of individual *Chlorella*. MMT as the formation sites of Pb(II)-bearing minerals rather than *Chlorella* results in more dispersed minerals on the surface of the *Chlorella*–MMT composite, both are conducive to decrease the bio-toxicity of Pb(II) and Pb(II)-bearing minerals. Additionally, the formation of stable phosphate minerals was observed in the presence of Ca(II) when ortho-P and pyro-P on the surface of *Chlorella* were hydrolyzed to $PO_4^{3-}$. In general, this study expands the knowledge of the clay–microbial consortium boosting Pb(II) bioremediation induced by *Chlorella* and demonstrated the mechanism of Pb(II) immobilization, providing a new insight into the bioremediation of Pb(II) in the soil of mining with high Ca(II) content.

## Data availability statement

The original contributions presented in the study are included in the article/Supplementary Material; further inquiries can be directed to the corresponding author.

## Author contributions

ZW: writing—original draft preparation, methodology, data curation, and investigation. JC: validation. JT: methodology, data curation, and investigation. ZL: writing—review and editing. XW: data curation. JL: writing—reviewing and editing, conceptualization, and supervision.

## Funding

This work was financially supported by the National Natural Science Foundation of China (Grant No. 32061123009).

## Acknowledgments

The authors thank their colleagues for providing technical assistance and scientific support, as well as their college and supervisors for providing analytical equipment.

## Conflict of interest

The authors declare that the research was conducted in the absence of any commercial or financial relationships that could be construed as a potential conflict of interest.

## Publisher's note



## Supplementary material

The Supplementary Material for this article can be found online at: https://www.frontiersin.org/articles/10.3389/fenvs.2022.983430/full#supplementary-material

# References

An, J.-H., and Dultz, S. (2008). Adsorption of Cr(VI) and as(V) on chitosan-montmorillonite: Selectivity and pH dependence. *Clays Clay Min.* 56, 549–557. doi:10.1346/CCMN.2008.0560508

Bhattacharyya, K. G., and Gupta, S. S. (2008). Adsorption of a few heavy metals on natural and modified kaolinite and montmorillonite: A review. *Adv. Colloid Interface Sci.* 140, 114–131. doi:10.1016/j.cis.2007.12.008

Bidanchi, R. M., Lalrindika, L., Khushboo, M., Bhanushree, B., Dinata, R., Das, M., et al. (2022). Antioxidative, anti-inflammatory and anti-apoptotic action of ellagic acid against lead acetate induced testicular and hepato-renal oxidative damages and pathophysiological changes in male Long Evans rats. *Environ. Pollut.* 302, 119048. doi:10.1016/j.envpol.2022.119048

Carfagna, S., Lanza, N., Salbitani, G., Basile, A., Sorbo, S., and Vona, V. (2013). Physiological and morphological responses of lead or cadmium exposed Chlorella sorokiniana 211-8K (Chlorophyceae). *SpringerPlus* 2, 147. doi:10.1186/2193-1801-2-147

Chen, M., Li, Y., Jiang, X., Zhao, D., Liu, X., Zhou, J., et al. (2021). Study on soil physical structure after the bioremediation of Pb pollution using microbial-induced carbonate precipitation methodology. *J. Hazard. Mat.* 411, 125103. doi:10.1016/j.jhazmat.2021.125103

Cheng, Y., Zhang, T., Chen, S., Li, F., Qing, R., Lan, T., et al. (2023). Unusual uranium biomineralization induced by green algae: Behavior investigation and mechanism probe. *J. Environ. Sci.* 124, 915–922. doi:10.1016/j.jes.2022.02.028

Cheng, Y., Zhang, T., Zhang, L., Ke, Z., Kovarik, L., and Dong, H. (2022). Resource recovery: Adsorption and biomineralization of cerium by *Bacillus licheniformis*. *J. Hazard. Mat.* 426, 127844. doi:10.1016/j.jhazmat.2021.127844

Cowley, J. M. (1956). Electron-diffraction study of the structure of basic lead carbonate, 2 $PbCO_3$. $Pb(OH)_2$. *Acta Crystallogr.* 9, 391–396. doi:10.1107/S0365110X56001133

Dhankhar, S., Bhalerao, G., Ganesamoorthy, S., Baskar, K., and Singh, S. (2017). Growth and comparison of single crystals and polycrystalline brownmillerite $Ca_2Fe_2O_5$. *J. Cryst. Growth* 468, 311–315. doi:10.1016/j.jcrysgro.2016.09.051

Figueiredo, N. M., Carvalho, N. J. M., and Cavaleiro, A. (2011). An XPS study of Au alloyed Al–O sputtered coatings. *Appl. Surf. Sci.* 257, 5793–5798. doi:10.1016/j.apsusc.2011.01.104

Gao, P. P., Zhang, X. M., Xue, P. Y., Dong, J. W., Dong, Y., Zhao, Q. L., et al. (2022). Mechanism of Pb accumulation in Chinese cabbage leaves: Stomata and trichomes regulate foliar uptake of Pb in atmospheric PM2.5. *Environ. Pollut.* 293, 118585. doi:10.1016/j.envpol.2021.118585

Hernandez-Garnica, M., García-García, R. J. D., Moreno-S anchez, R., and Sanchez-Thomas, R. (2021). Lead accumulation in photosynthetic Euglena gracilis depends on polyphosphates and calcium. *Environ. Pollut.* 272, 116007. doi:10.1016/j.envpol.2020.116007

Huang, R., Huo, G., Song, S., Li, Y., Xia, L., and Gaillard, J. F. (2019). Immobilization of mercury using high-phosphate culture-modified microalgae. *Environ. Pollut.* 254, 112966. doi:10.1016/j.envpol.2019.112966

Ibrahim, A. A., Adel, A. M., El–Wahab, Z. H. A., and Al–Shemy, M. T. (2011). Utilization of carboxymethyl cellulose based on bean hulls as chelating agent. Synthesis, characterization and biological activity. *Carbohydr. Polym.* 83, 94–115. doi:10.1016/j.carbpol.2010.07.026

Ivanina, A. V., Jarrett, A., Bell, T., Rimkevicius, T., Beniash, E., and Sokolova, I. M. (2020). Effects of seawater salinity and pH on cellular metabolism and enzyme activities in biomineralizing tissues of marine bivalves. *Comp. Biochem. Physiology Part A Mol. Integr. Physiology* 248, 110748. doi:10.1016/j.cbpa.2020.110748

Jiang, L., Sun, H., Peng, T., Ding, W., Liu, B., and Liu, Q. (2021). Comprehensive evaluation of environmental availability, pollution level and leaching heavy metals behavior in non-ferrous metal tailings. *J. Environ. Manage.* 290, 112639. doi:10.1016/j.jenvman.2021.112639

Kang, J. H., Han, J., Lee, H., Lim, M. H., Kim, K.-T., and Kim, C. (2018). A water-soluble fluorescence chemosensor for the sequential detection of $Zn^{2+}$ and pyrophosphate in living cells and zebrafish. *Dyes Pigm.* 152, 131–138. doi:10.1016/j.dyepig.2018.01.039

Koloren, O., Koloren, Z., and Eker, S. (2016). Molecular phylogeny of Artemisia species based on the internal transcribed spacer (ITS) of 18S-26S rDNA in Ordu Province of Turkey. *Biotechnol. Biotechnol. Equip.* 30, 929–934. doi:10.1080/13102818.2016.1188674

Krishnamoorthy, R., Govindan, B., Banat, F., Sagadevan, V., Purushothaman, M., and Show, P. L. (2019). Date pits activated carbon for divalent lead ions removal. *J. Biosci. Bioeng.* 128, 88–97. doi:10.1016/j.jbiosc.2018.12.011

Kumar, A., and Lingfa, P. (2020). Sodium bentonite and kaolin clays: Comparative study on their FT-IR, XRF, and XRD. *Mater. Today Proc.* 22, 737–742. doi:10.1016/j.matpr.2019.10.037

Lee, S. Y., Jung, K. H., Lee, J. E., Lee, K. A., Lee, S. H., Lee, J. Y., et al. (2014). Photosynthetic biomineralization of radioactive Sr via microalgal CO2 absorption. *Bioresour. Technol.* 172, 449–452. doi:10.1016/j.biortech.2014.09.023

Li, F., Wang, W., Li, C., Zhu, R., Ge, F., Zheng, Y., et al. (2018). Self-mediated pH changes in culture medium affecting biosorption and biomineralization of Cd(2+) by Bacillus cereus Cd01. *J. Hazard. Mat.* 358, 178–186. doi:10.1016/j.jhazmat.2018.06.066

Li, G. L., Zhou, C. H., Fiore, S., and Yu, W. H. (2019). Interactions between microorganisms and clay minerals: New insights and broader applications. *Appl. Clay Sci.* 177, 91–113. doi:10.1016/j.clay.2019.04.025

Li, J., Li, Z., Brandis, K. J., Bu, J., Sun, Z., Yu, Q., et al. (2020). Tracing geochemical pollutants in stream water and soil from mining activity in an alpine catchment. *Chemosphere* 242, 125167. doi:10.1016/j.chemosphere.2019.125167

Li, X., Yang, C., Lin, Y., Hu, T., and Zeng, G. (2022). Effects of oxytetracycline and zinc ion on nutrient removal and biomass production via microalgal culturing in anaerobic digester effluent. *Bioresour. Technol.* 346, 126667. doi:10.1016/j.biortech.2021.126667

Li, Y., Song, S., Xia, L., Yin, H., García Meza, J. V., and Ju, W. (2019). Enhanced Pb(II) removal by algal-based biosorbent cultivated in high-phosphorus cultures. *Chem. Eng. J.* 361, 167–179. doi:10.1016/j.cej.2018.12.070

Liu, M., Zhao, L., Liu, Y., Lan, Z., Chang, L., Li, Y., et al. (2014). Role of heavy metal ions in the formation of oxyfluoride glasses and glass ceramics. *J. Mater. Sci. Technol.* 30 (30), 1213–1216. doi:10.1016/j.jmst.2014.02.003

Liu, X., Cao, J., Li, Y., Hu, G., and Wang, G. (2019). A study of metal-bearing nanoparticles from the Kangjiawan Pb-Zn deposit and their prospecting significance. *Ore Geol. Rev.* 105, 375–386. doi:10.1016/j.oregeorev.2018.12.025

Ma, Y., Shen, W., Tang, T., Li, Z., and Dai, R. (2022). Environmental estrogens in surface water and their interaction with microalgae: A review. *Sci. Total Environ.* 807, 150637. doi:10.1016/j.scitotenv.2021.150637

Miler, M., Bavec, S., and Gosar, M. (2022). The environmental impact of historical Pb-Zn mining waste deposits in Slovenia. *J. Environ. Manage.* 308, 114580. doi:10.1016/j.jenvman.2022.114580

Nzaba Madila, E. E., Rousselot, S., Rioux, M., Dollé, M., and Duong, A. (2022). Comparative studies of synthesis, structure, optical properties and conductivity of the monoclinic phases $Na_2Co_6Mn_2(PO_4)_6$ and $Na_2Co_6Ni_2(PO_4)_6$. *Solid State Sci.* 124, 106779. doi:10.1016/j.solidstatesciences.2021.106779

Obiri-Yeboah, A., Nyantakyi, E. K., Mohammed, A. R., Yeboah, S. I. I. K., Domfeh, M. K., and Abokyi, E. (2021). Assessing potential health effect of lead and mercury and the impact of illegal mining activities in the Bonsa river, Tarkwa Nsuaem, Ghana. *Sci. Afr.* 000, e00876. doi:10.1016/j.sciaf.2021.e00876

Osorio-Yanez, C., Sanchez-Guerra, M., Solano, M., Baccarelli, A., Wright, R., Sanders, A. P., et al. (2021). Metal exposure and bone remodeling during pregnancy: Results from the PROGRESS cohort study. *Environ. Pollut.* 282, 116962. doi:10.1016/j.envpol.2021.116962

Priyanka, N., Geetha, N., Manish, T., Sahi, S. V., and Venkatachalam, P. (2021). Zinc oxide nanocatalyst mediates cadmium and lead toxicity tolerance mechanism by differential regulation of photosynthetic machinery and antioxidant enzymes level in cotton seedlings. *Toxicol. Rep.* 8, 295–302. doi:10.1016/j.toxrep.2021.01.016

Qian, T. T., Li, D. C., and Jiang, H. (2014). Thermochemical behavior of tris(2-butoxyethyl) phosphate (TBEP) during co-pyrolysis with biomass. *Environ. Sci. Technol.* 48, 10734–10742. doi:10.1021/es502669s

Rahman, Z., and Singh, V. P. (2020). Bioremediation of toxic heavy metals (THMs) contaminated sites: Concepts, applications and challenges. *Environ. Sci. Pollut. Res.* 27, 27563–27581. doi:10.1007/s11356-020-08903-0

Rajasekar, A., Wilkinson, S., and Moy, C. K. S. (2021). MICP as a potential sustainable technique to treat or entrap contaminants in the natural environment: A review. *Environ. Sci. Ecotechnology* 6, 100096. doi:10.1016/j.ese.2021.100096

Saisopa, T., Klaiphet, K., Songsiriritthigul, P., Pokapanich, W., Tangsukworakhun, S., Songsiriritthigul, C., et al. (2020). Investigation of solvated calcium dication structure in pure water, methanol, and ethanol solutions by means of K and L2, 3-edges X-ray absorption spectroscopy. *J. Electron Spectros. Relat. Phenom.* 244, 146984. doi:10.1016/j.elspec.2020.146984

Samsudin, A. S., and Saadiah, M. A. (2018). Ionic conduction study of enhanced amorphous solid bio-polymer electrolytes based carboxymethyl cellulose doped $NH_4Br$. *J. Non-Crystalline Solids* 497, 19–29. doi:10.1016/j.jnoncrysol.2018.05.027

Senn, D. B., Estes, E. R., Brabander, D. J., and Shine, J. P. (2014). Sources and fates of heavy metals in a mining-impacted stream: Temporal variability and the role of iron oxides. *Sci. Total Environ.* 490, 456–466. doi:10.1016/j.scitotenv.2014.04.126

Shan, B., Hao, R., Xu, H., Li, J., Li, Y., Xu, X., et al. (2021). A review on mechanism of biomineralization using microbial-induced precipitation for immobilizing lead ions. *Environ. Sci. Pollut. Res. Int.* 28, 30486–30498. doi:10.1007/s11356-021-14045-8

Slaveykova, V. I., and Wilkinson, K. J. (2003). Effect of pH on Pb biouptake by the freshwater alga *Chlorella kesslerii*. *Environ. Chem. Lett.* 1, 185–189. doi:10.1007/s10311-003-0041-8

Su, M., Han, F., Wang, M., Ma, J., Wang, X., Wang, Z., et al. (2021). Clay-assisted protection of *Enterobacter sp.* from Pb (II) stress. *Ecotoxicol. Environ. Saf.* 208, 111704. doi:10.1016/j.ecoenv.2020.111704

Tan, J., Yi, H., Zhang, Z., Meng, D., Li, Y., Xia, L., et al. (2022). Montmorillonite facilitated Pb(II) biomineralization by *Chlorella sorokiniana* FK in soil. *J. Hazard. Mat.* 423, 127007. doi:10.1016/j.jhazmat.2021.127007

Tang, Q., Katsumi, T., Inui, T., and Li, Z. (2015). Influence of pH on the membrane behavior of bentonite amended Fukakusa clay. *Sep. Purif. Technol.* 141, 132–142. doi:10.1016/j.seppur.2014.11.035

Ummalyma, S. B., and Singh, A. (2022). Biomass production and phycoremediation of microalgae cultivated in polluted river water. *Bioresour. Technol.* 351, 126948. doi:10.1016/j.biortech.2022.126948

Wang, J., Rosov, T., Wensel, P., McGowen, J., and Curtis, W. R. (2016). A preliminary implementation of metabolic-based pH control to reduce $CO_2$ usage in outdoor flat-panel photobioreactor cultivation of Nannochloropsis oceanica microalgae. *Algal Res.* 18, 288–295. doi:10.1016/j.algal.2016.07.001

Wang, M., Wu, S., Guo, J., Liao, Z., Yang, Y., Chen, F., et al. (2021). Immobilization and migration of arsenic during the conversion of microbially induced calcium carbonate to hydroxylapatite. *J. Hazard. Mater.* 412, 125261. doi:10.1016/j.jhazmat.2021.125261

Wang, P., Sun, Z., Hu, Y., and Cheng, H. (2019). Leaching of heavy metals from abandoned mine tailings brought by precipitation and the associated environmental impact. *Sci. Total Environ.* 695, 133893. doi:10.1016/j.scitotenv.2019.133893

Winning, L. D., Gorczyca, B., and Brezinski, K. (2017). Effect of total organic carbon and aquatic humic substances on the occurrence of lead at the tap. *Water Qual. Res. J.* 52, 2–10. doi:10.2166/wqrjc.2017.028

Wu, W., Qu, S., Nel, W., and Ji, J. (2020). The impact of natural weathering and mining on heavy metal accumulation in the karst areas of the Pearl River Basin, China. *Sci. Total Environ.* 734, 139480. doi:10.1016/j.scitotenv.2020.139480

Wu, Y., Wang, Y., Du, J., Wang, Z., and Wu, Q. (2016). Effects of yttrium under lead stress on growth and physiological characteristics of Microcystis aeruginosa. *J. Rare Earths* 34, 747–756. doi:10.1016/S1002-0721(16)60089-3

Xu, Q., Gao, Y., Wu, X., Ye, J., Ren, X., Zhou, Z., et al. (2021). Derivation of empirical model to predict the accumulation of Pb in rice grain. *Environ. Pollut.* 274, 116599. doi:10.1016/j.envpol.2021.116599

Yang, B., Shan, J., Xing, F., Dai, X., Wang, G., Ma, J., et al. (2022). Distribution, accumulation, migration and risk assessment of trace elements in peanut-soil system. *Environ. Pollut.* 304, 119193. doi:10.1016/j.envpol.2022.119193

Yu, X., Jiang, J., Liu, J., and Li, W. (2021). Review on potential uses, cementing process, mechanism and syntheses of phosphate cementitious materials by the microbial mineralization method. *Constr. Build. Mater.* 273, 121113. doi:10.1016/j.conbuildmat.2020.121113

Zeng, Q., Zhu, T., Wen, Y., Li, F., Cheng, Y., Chen, S., et al. (2022). The dynamic behavior and mechanism of uranium (VI) biomineralization in *Enterobacter sp.* X57. *Chemosphere* 298, 134196. doi:10.1016/j.chemosphere.2022.134196

Zeng, X., Xu, X., Boezen, H. M., and Huo, X. (2016). Children with health impairments by heavy metals in an e-waste recycling area. *Chemosphere* 148, 408–415. doi:10.1016/j.chemosphere.2015.10.078

Zhang, H. Y., Xia, Y. M., Liu, X. J., and Li, T. D. (2013). Research on influence of diffractometer slits on XRD pattern. *Key Eng. Mat.* 544, 441–444. doi:10.4028/www.scientific.net/kem.544.441

Zhang, M., Zhang, T., Zhou, L., Lou, W., Zeng, W., Liu, T., et al. (2022). Soil microbial community assembly model in response to heavy metal pollution. *Environ. Res.* 213, 113576. doi:10.1016/j.envres.2022.113576

Zhu, Y., Feng, W., Liu, S., He, Z., Zhao, X., Liu, Y., et al. (2018). Bioavailability and preservation of organic phosphorus in lake sediments: Insights from enzymatic hydrolysis and (31)P nuclear magnetic resonance. *Chemosphere* 211, 50–61. doi:10.1016/j.chemosphere.2018.07.134